Nanoscale Advances

ROYAL SOCIETY OF CHEMISTRY

PAPER

View Article Online
View Journal | View Issue

Cite this: *Nanoscale Adv.*, 2025, **7**, 6646

Synthesis of carbon quantum dots based on hemp leaves and cysteamine for latent fingerprint detection and their potential therapeutic anticancer application

Ratchaneekorn Kampangta,[a] Apichart Saenchoopa,[a] Waranya Obrom,[a] Wonn Shweyi Thet Tun,[b] Chatchai Muanprasat,[c] Kazuhiko Maeda,[de] Pornsiri Suwannapaporn,[c] Chomponoot Suppaso,[d] Wasan Seemakram,[f] Sophon Boonlue[g] and Sirinan Kulchat *[a]

Received 21st March 2025
Accepted 22nd August 2025

DOI: 10.1039/d5na00264h

rsc.li/nanoscale-advances

In this study, an eco-friendly one-pot hydrothermal method was used to synthesize carbon quantum dots (CQDs) using hemp leaves and cysteamine hydrochloride as the carbon and nitrogen-sulfur sources, respectively. Synthesized carbon quantum dots (HC-CQDs) were developed to achieve the clear detection of latent fingerprints (LFPs) on non-porous materials under UV-light, and their nontoxicity to humans was verified by testing on cancer cells. HC-CQDs characterized by various techniques exhibited a high quantum yield of 36.1%, and their excitation and emission peaks appeared at 354 and 434 nm, respectively. For the detection of LFPs, we prepared a fluorescence fingerprint powder utilizing HC-CQDs, cellulose nanofiber (CNF), chitosan, and cassava starch. Results showed a complete fingerprint, and it was possible to clearly identify the location and type of defects on the fingerprint (minutiae). Additionally, we performed MTT assays to understand the effect of HC-CQDs on cell viability in cancer cell lines. HC-CQDs exhibited pronounced anti-cancer activity against A549 lung carcinoma cells while demonstrating negligible cytotoxic effects on normal Vero cells. Therefore, this study successfully developed plant-based fluorescent carbon quantum dots, which can be used to prepare a fluorescent powder for detecting LFPs that is safe for forensic scientists. These HC-CQDs also possess potential in inhibiting A549 lung cancer cells, which could be further developed in the medical field.

1. Introduction

Carbon quantum dots (CQDs) are a novel group of zero-dimensional carbon nanoparticles that predominantly consist of carbon and possess sizes smaller than 10 nm.[1] In recent years, significant focus has been directed towards carbon quantum dots owing to their distinctive physiochemical characteristics, including low toxicity, stable photoluminescence, water solubility, adaptability for surface modification, resilience against photobleaching, and emission that depends on the excitation wavelength.[2] Among the optical properties of CQDs, photoluminescence (PL), encompassing fluorescence and phosphorescence, is particularly intriguing. At present, there are many strategies focused on improving the luminescence efficiency of CQDs, such as controlling the particle size and shape, surface passivation, doping with heteroatoms, and optimization of the synthesis conditions.[3] CQDs synthesis can be accomplished in several ways, which are typically divided into two main categories: top-down and bottom-up approaches. Hydrothermal method has emerged as the most captivating approach due to its uncomplicated operation and facile control during the reaction. In addition, it is an eco-friendly, easy to handle, and impregnable route to synthesize CQDs from natural carbon-based precursors.[4]

Hemp, scientifically known as *Cannabis sativa* L. and belonging to the Cannabaceae family, is an age-old cultivated plant that originated in central Asia.[5] The use of hemp leaves as CQD precursors represents a cost-effective and environmentally

[a]*Center of Excellence for Innovation in Chemistry and Materials Chemistry Research Center, Department of Chemistry, Faculty of Science, Khon Kaen University, Khon Kaen, 40002, Thailand. E-mail: sirikul@kku.ac.th*

[b]*Department of System Biosciences and Computational Medicine, Faculty of Medicine, Khon Kaen University, Khon Kaen, 40002, Thailand*

[c]*Chakri Naruebodindra Medical Institute, Faculty of Medicine Ramathibodi Hospital, Mahidol University, Thailand*

[d]*Department of Chemistry, School of Science, Institute of Science Tokyo, 2-12-1-NE-2 Ookayama, Meguro-ku, Tokyo 152-8550, Japan*

[e]*Research Center for Autonomous Systems Materialogy (ASMat), Institute of Science Tokyo, 4259 Nagatsuta-cho, Midori-ku, Yokohama, Kanagawa 226-8501, Japan*

[f]*Department of Microbiology and Parasitology, Faculty of Medical Science, Naresuan University, 65000, Thailand*

[g]*Department of Microbiology, Faculty of Science, Khon Kaen University, Khon Kaen, 40002, Thailand*

friendly approach to utilize natural resources. Scientists need to study different plant species to create nanomaterials that show better optical properties for industrial applications. While various plant materials have been explored for CQDs synthesis, hemp leaves offer unique advantages as a precursor due to their rich composition of bioactive compounds, particularly cannabinoids and terpenes, which can potentially enhance the functional properties of the resulting CQDs. Additionally, hemp's widespread availability, rapid growth cycle, and minimal cultivation requirements make it an economically viable and sustainable choice for large-scale CQD production.[6,7] One of the most well-known groups of compounds in hemp is cannabinoids, which include compounds like tetrahydrocannabinol (THC), cannabidiol (CBD), and cannabinoid (CBN).[8] These cannabinoids are primarily found in the resin of the hemp leaves. Nevertheless, in recent times, most nations have embraced the legalization of industrial hemp production, leading to a surge in research efforts focusing on the potential health advantages of hemp and its derived products. It is important to note that current investigations are still underway to substantiate the diverse health claims associated with the vast array of commercially available hemp products.[9] Cysteamine hydrochloride is a dopant comprising N and S, which helps to increase the fluorescence intensity of CQDs and is beneficial for displaying the high quantum yield and photostability of CQDs.[10]

The dual functionality of our HC-CQDs in both forensic analysis and therapeutic applications represents a novel approach in materials science. This unique combination stems from the CQDs' distinct photoluminescent properties, which enable highly sensitive fingerprint detection, while their biocompatibility and cellular interactions make them promising candidates for targeted cancer therapy. The integration of these seemingly disparate applications in a single material system offers significant advantages in terms of cost-effectiveness and versatility. Latent fingerprints (LFPs) are a type of fingerprint that is not immediately visible to the naked eye. Sweat, natural oils, and other residues on the skin cause LFPs on materials. At a crime scene, LFPs are one of the most valuable types of evidence for identifying suspects or reconstructing events, which may be found on many materials such as paper, glass, doorknobs, metal sheets, plastic sheets, wood, banknotes, and others.[11,12] One popular method for detecting LFPs is powder dusting, which is considered a simple and convenient method with no complicated steps and not dangerous to users.[13] Dusting for fingerprints is a common forensic technique used to reveal LFPs on smooth, non-porous surfaces like glass, plastic, or metal. This process highlights prints left by the natural oils and sweat on the fingertips, making them visible for collection and analysis.[14] Recently, fluorescent dust has been considered more frequently for use in forensic science because it produces more visible fingerprints than non-fluorescent dust and stimulates repeated fluorescence.[15] However, the expensive cost of fluorescent powder and the requirement to import it from overseas place a limit on its utilization. Therefore, the production of fluorescent powders for LFP detection using CQDs, which are cost-effective and synthesized from natural materials, may be beneficial to the forensic science industry.

Cell viability assays are essential in studying the effects of treatments on cancer cell lines, particularly to assess how various drugs, radiation, or genetic modifications impact cell survival. Viability assays generally indicate the number of live cells post-treatment, helping to determine the cytotoxic effects and therapeutic potential of interventions. CQDs have been demonstrated as an effective instrument for imaging, medicinal, and sensing applications.[16] Pourmadadi *et al.*[17] used CQDs as a component in the preparation of a pH-sensitive nanocarrier for quercetin (QC) delivery to A549 lung cancer. *In vitro* cytotoxicity and cell death were investigated using MTT analysis. Choppadandi *et al.*[18] prepared amine-functionalized carbon quantum dots (A-CQDs) and then covalently conjugated them with magnetic nanoparticles (MNPs) to form a single nanosystem for the combinational therapy of cancer cells. Research results showed that the combinational therapy is highly effective towards A549 cells treatment. Their beneficial qualities, such as their high brightness, have sparked a strong interest in using them as labels in bioanalytical applications.[19] CQDs can be used to tag cells with receptor types on their surfaces in pathology investigations to identify malignant cells and show whether the tumor is amenable to the targeted therapy.[20]

In this work, we suggest a new strategy that leverages the unique properties of HC-CQDs for both forensic and therapeutic applications, and Scheme 1 represents the full scope of our work. By incorporating cysteamine hydrochloride as a surface modifier, we enhance both the fluorescent properties for fingerprint detection and the biocompatibility for cancer cell targeting. We aimed to develop HC-CQDs for highly fluorescent powders and their application in targeting anti-lung cancer cells. Hemp and cysteamine hydrochloride were used as the carbon source and thiol-reagent with $-NH_2$ and –SH at the end of the molecule, respectively, while deionized water was used as the reaction solvent to prepare carbon quantum dots through an eco-friendly hydrothermal method.

2. Materials and methods

2.1 Chemicals and materials

The Department of Microbiology, Faculty of Science, Mycorrhiza and Mycotechnology Laboratory, Khon Kaen University, Thailand, is where the hemp leaves were acquired. Sigma-Aldrich, Thailand, supplied the bioreagent ≥98.0% quinine hemisulfate salt monohydrate ($C_{20}H_{24}N_2O_2 \cdot 0.5H_2O_4S \cdot H_2O$, suitable for fluorescence), and ≥98.0% cysteamine hydrochloride (C_2H_8ClNS). Acetic acid (CH_3COOH) and 98% sulfuric acid (H_2SO_4) were purchased from RCI Labscan, Thailand. Deionized (DI) water was produced using a Millipore water filtration system, RiOs TM Type I Simplicity 185. Department of Chemistry, Khon Kaen University, Thailand's Inorganic Laboratory, is where the cellulose nanofiber (CNF) was acquired. In Khon Kaen, Thailand, commercial tapioca flour (Five Stars Fish brand) was bought from a nearby grocery.

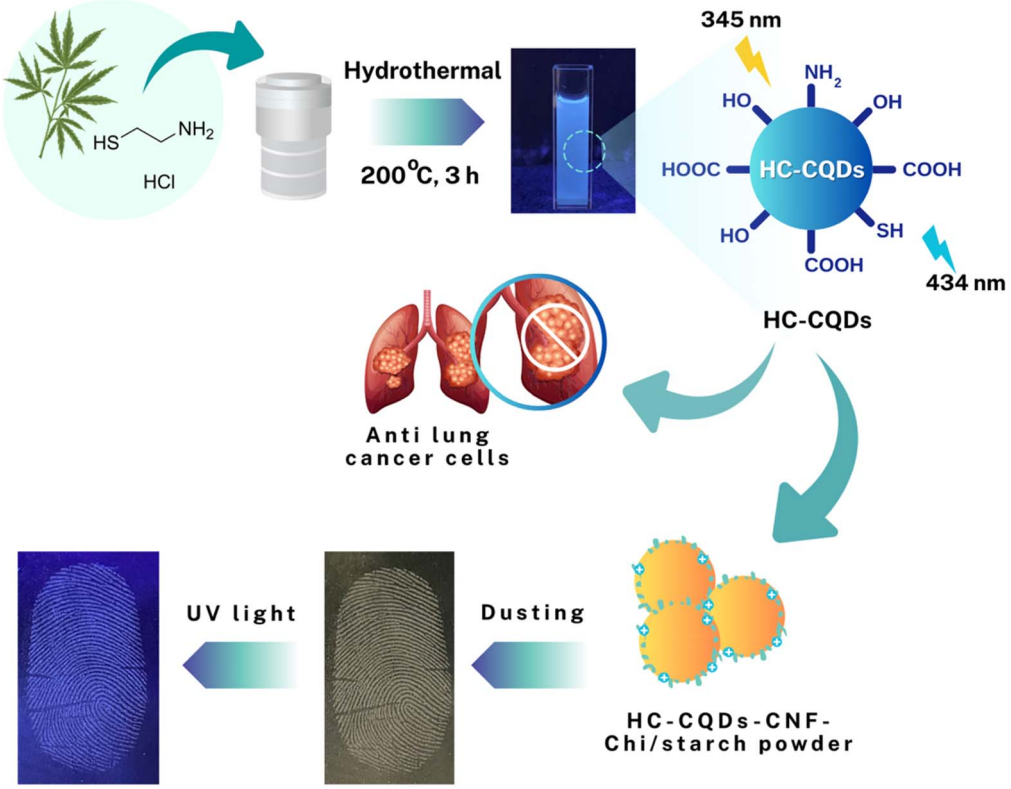

Scheme 1 Synthesis of HC-CQDs, which were utilized to detect LFPs and can be possibly used against lung cancer cells.

2.2 Instruments

Absorption spectra, emission spectra and relative quantum yield measurements of HC-CQDs were determined using a Cary 60 UV-Vis Agilent Technologies and FS5 Edinburgh instruments spectrofluorometer, respectively. The morphology and particle size were observed by TEM, Talos F200X, Netherlands. The vibrational spectra were examined using FT-IR, Bruker model TENSOR 27 spectrometers. The lattice spacing was verified by HRTEM, Talos F200X, Netherlands. Crystal structures were determined *via* XRD, Bruker, D8 Advance. The chemical composition was observed by XPS, Shimadzu ESCA-3400 spectrometer, Mg anode. The elemental components were observed by EDX, Talos F200X, Netherlands. The size distribution profiles in solution were verified by DLS, Malvern, England, Model: Zetasizer Nano ZS. Synthesis of HC-CQDs was achieved by hydrothermal method using the UN55 hot air oven from the Memmert company.

2.3 Synthesis of carbon quantum dots (HC-CQDs) and HC-CQDs-CNF-Chi/starch powder

The typical synthesis of CQDs began with hemp extraction; 1 g of hemp leaves powder was dissolved in 50 mL of DI water. Then, the mixture solution was stirred under magnetic stirring and heated at 60 °C for 1 hour. Finally, the sample underwent air-cooling to room temperature and was filtered using No. 1 Whatman filter paper. The extracted hemp solution was kept in the refrigerator. First, 0.01 g of cysteamine hydrochloride was dissolved in 10 mL of hemp extract solution. After being transferred to a stainless-steel autoclave, the mixture was baked for 3 hours at 200 °C in the oven. The mixture spontaneously cooled to room temperature following the reaction. Then, it was purified to eliminate larger aggregates or residues by centrifuging at 8000 rpm for 15 minutes and filtering through 0.22 μm nylon filters, respectively. Finally, the yellowish-brown solution (HC-CQDs) was collected and stored in dark bottles.

To make HC-CQDs-CNF-Chi/starch powder, 0.05 g of cellulose nanofiber (CNF) was dissolved in 20 mL of HC-CQDs solution under magnetic stirring. Then, 10 mL of 0.5%(w/v) chitosan (in 0.1%(v/v) CH_3COOH) was slowly added. Lastly, added 5 g of tapioca starch was combined with the mixture solution with continuous stirring at room temperature for 24 hours. The mixture was dried at 60 °C for 24 hours. The dried HC-CQDs-CNF-Chi/starch powder was sieved using a stainless-steel mesh (150 mesh size) to ensure uniform particle size distribution and remove large agglomerates or unprocessed residues. Finally, the powder was thoroughly ground into a fine consistency and collected at room temperature.

2.4 Detection of latent fingerprints on non-porous surfaces under UV light

The application of HC-CQDs was investigated as a fluorescent powder for LFP detection using the common dusting method. An LFP sample was collected from a 25 year old woman volunteer's thumb with her consent on surfaces made of various materials for 3 seconds at ambient temperature. On the fingerprint, the HC-CQDs-CNF-Chi/starch powder was applied

by dusting method and exposed to UV light at 365 nm in a closed room. Finally, LFP images were obtained using a smartphone (iPhone 12) as the signal collector.

2.5 Cell culture for studying the effect of HC-CQDs on cell viability in cancer cell lines

The Collection of American Type Culture (Manassas, VA, USA) provided the A549 lung adenocarcinoma cells, SCC head and neck squamous carcinoma cells, LS174T colorectal cancer cells, and Vero kidney epithelium cells (normal cells). The Kaighn's Modification of Ham's F-12 Medium (F-12k) with 10% fetal bovine serum (FBS) and 100 U per mL penicillin (Life Technologies, Carlsbad, CA, USA) was used to sustain the A549 cells. Dulbecco's Modified Eagle Medium/Ham's F-12 (DMEMF-12) containing 10% FBS and 100 U per mL penicillin was used to sustain the SCC cells. A RPMI-1640 supplemented with 10% FBS and 100 U per mL penicillin was used to sustain the LS174T cells. Eagle's Minimum Essential Medium (EMEM) with 10% FBS and 100 U per mL penicillin was used to sustain the Vero cells. Each cell culture was kept in an atmosphere that was humidified with 95% oxygen and 5% carbon dioxide at 37 °C.

2.6 MTT assay

MTT (3-[4,5-dimethylthiazol-2-yl]-2,5 diphenyl tetrazolium bromide) assays were used to evaluate cell viability.[21] Briefly, A549 cells (5000 cells per well), SCC cells (10 000 cells per well), and Vero cells (4000 cells per well) were seeded in 96-well plates and incubated at 37 °C for 24 hours. LS174T was seeded in 96-well plates (7000 cells per well) and incubated at 37 °C for 48 hours. After incubation, the cells were treated with different concentrations of HC-CQDs for 48 and 72 hours. The MTT solution (5 mg mL^{-1}) was added to the medium and incubated at 37 °C for 2 hours. The absorbance of each sample was measured at 570 nm using a Synergy Neo2 Multi-Mode Microplate Reader (BioTek Instruments, VT, USA). Control groups consisted of A549 cells, SCC cells, LS174T cells, and Vero cells that were not treated with HC-CQDs.

3. Results and discussion

3.1 UV-visible absorption and photoluminescence property

The optical properties of the synthesized HC-CQDs were first characterized by UV-vis absorption and fluorescence spectroscopy. The absorption spectrum shows a slight absorption band at 250 nm corresponding to π–π* transitions of C=C bonds in the aromatic sp^2 domains of HC-CQDs, and an insignificant absorption peak at 350 nm consistent with n–π* transitions of the C=O bonds.[22] The maximum emission intensity of the peaks of HC-CQDs appears at 434 nm when excited at 345 nm (Fig. 1a). This indicates that the maximum radiative recombination efficiency occurs at this excitation wavelength, which corresponds to the optimal excitation-emission pairing for the material caused by quantum confinement effects from varied HC-CQD sizes which influence the PL behavior. Smaller particles emit at shorter wavelengths due to larger bandgaps, while larger ones emit at longer wavelengths, as different sizes may be preferentially excited at different wavelengths.[23,24] To investigate the effect of adding cysteamine hydrochloride on the luminescence efficiency of the carbon quantum dots, we measured the photoluminescence (PL) intensity of three types: H-CQDs, C-CQDs, and HC-CQDs. The PL spectra showed the fluorescence intensity increases in the order: C-CQDs < H-CQDs < HC-CQDs (Fig. S1a). The low intensity of C-CQDs likely results from their minimal carbon content (present in cysteamine hydrochloride), leading to fewer carbon quantum dot particles. In contrast, H-CQDs use hemp extract as a carbon source, explaining their higher intensity. Similarly, HC-CQDs exhibit the highest intensity, indicating that adding cysteamine hydrochloride enhances the luminescence efficiency of the carbon quantum dots. These results support the idea that doping with N and S heteroatoms on the carbon quantum dot surface increases the fluorescence intensity.[25]

In Fig. 1b, the emission intensity of HC-CQDs demonstrated a clear dependence on the excitation wavelength, gradually increasing from 325 nm to 345 nm and subsequently decreasing

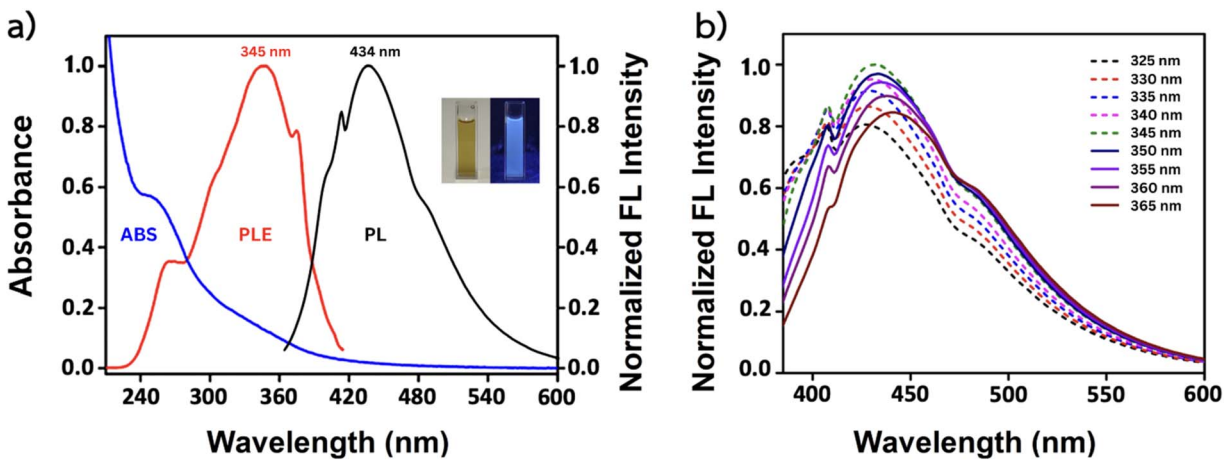

Fig. 1 (a) UV-vis absorption (blue curve), PL excitation (red curve), and PL emission spectra (black curve) of HC-CQDs (inset: pictures of HC-CQDs in ambient (left) and UV light (right)). (b) Emission spectra of HC-CQDs recorded under excitation wavelengths ranging from 325 to 365 nm.

as the excitation was further extended to 365 nm. As the excitation wavelength increases, selective activation of these states causes a redshift and reduced PL intensity, typical in heterogeneously structured CQDs. This phenomenon can be attributed to the surface defects and oxygen-containing groups on HC-CQDs creating multiple emissive trap states that contribute to excitation-dependent emission.[26] Notably, the emission spectra exhibit two distinct shoulder peaks, which can be attributed to multiple emission centers within HC-CQDs. The first shoulder peak around 425 nm likely originates from the intrinsic carbon core states, while the second shoulder peak around 450 nm may be associated with surface states created by the N, S co-doping from cysteamine functionalization. This dual-emission characteristic suggests the presence of multiple radiative recombination pathways, commonly observed in heteroatom-doped CQDs.[27] Heteroatom doping can greatly enhance the quantum yield (QY) of carbon quantum dots. In synthesized HC-CQDs, N and S doping may provide effective enhancement and exhibit relatively high QY.[28] The QY of HC-CQDs with 2.55×10^{-4} M quinine sulfate in 0.1 N H_2SO_4 was utilized as a reference material, demonstrating a QY of 54.6% at 450 nm. The QY of HC-CQDs can be calculated using the following equation:[29]

$$\phi_S = \phi_R(\mathrm{Grad}_S/\mathrm{Grad}_R)(n_S/n_R)2 \quad (1)$$

where ϕ_S and ϕ_R are the quantum yields of HC-CQDs and quinine sulfate, Grad_S and Grad_R are the gradients calculated from the integrated fluorescence intensity *vs.* absorbance plot of HC-CQDs and quinine sulfate, and n_S and n_R are refractive indexes of HC-CQDs and quinine sulfate, respectively. The results of this experiment shown in Fig. S2 exhibit a great FL quantum yield of 36.1%, which is much better than that observed in other works that synthesized carbon quantum dots from natural materials, as shown in Table S1.[30–36]

3.2 Morphological and functional group analysis

The morphology and particle sizes of HC-CQDs were observed by TEM. Fig. 2a illustrates the spherical and well-dispersed HC-CQDs. The distribution of the particle sizes, as shown in Fig. 2b, ranges from 14.6 to 40.3 nm with an average diameter of 27.4 ± 5.3 nm. The size of the CQDs may be controlled *via* the hydrothermal synthesis process. According to the identification of HC-CQDs produced, aggregation may cause the size of the CQDs to exceed 10 nm in certain instances.[37] According to Table S2, the zeta potential approach for examining the hydrodynamic size of HC-CQDs indicates a size of 278.6 ± 14.2 nm, which could involve the encapsulation of water or other substances, resulting in a greater particle size for HC-CQDs than that determined by TEM. The difference between the TEM and DLS measurements is commonly observed in nanoparticles characterization. This discrepancy can be attributed to several factors as TEM measures the physical size of the dried particles in vacuum, while DLS measures the hydrodynamic diameter of particles in solution, including their hydration shell and any surface-bound molecules.[38,39] Moreover, the presence of

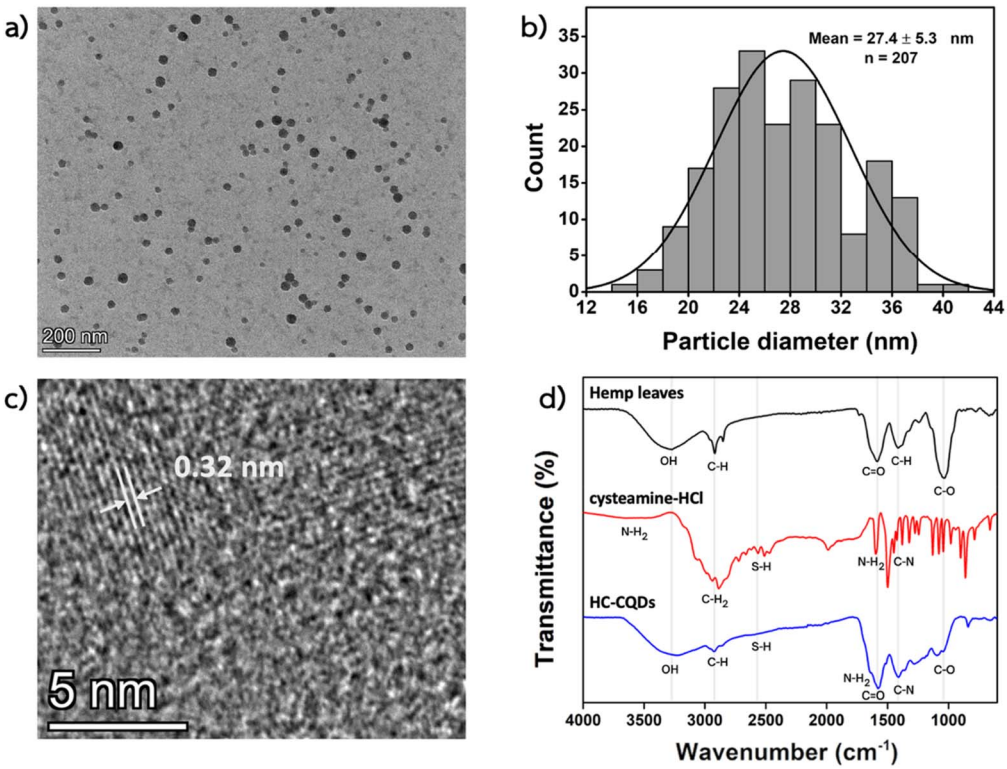

Fig. 2 (a) TEM image of HC-CQDs; (b) particle size distribution of HC-CQDs; (c) HR-TEM image of HC-CQDs; and (d) FT-IR spectra of raw hemp, cysteamine-HCl, and synthesized HC-CQDs.

cysteamine surface modification and potential aggregation in solution can increase the effective hydrodynamic size.[40] The larger hydrodynamic diameter suggests successful surface functionalization, and indicates that HC-CQDs may form small clusters in aqueous solution while maintaining their individual particle integrity as observed in TEM.[40] The *d*-spacing value of HC-CQDs obtained by HR-TEM is shown in Fig. 2c. It was shown that HC-CQDs had a lattice spacing of 0.32 nm, which indicate a graphitic interlayer spacing, as shown by the (002) graphitic carbon.[41,42]

The FT-IR spectra (Fig. 2d) show that functional groups on the HC-CQD surface originate from both hemp and cysteamine hydrochloride. In the hemp spectrum, there are peaks at 3269 cm^{-1} (O–H stretching), 2918 cm^{-1} (C–H stretching), 1584 cm^{-1} (C═O stretching), 1412 cm^{-1} (C–H bending), and 1032 cm^{-1} (C–O stretching).[43,44] The spectrum of cysteamine hydrochloride shows peaks at 3637 cm^{-1} (N–H stretching of the amino group), 2886 cm^{-1} (C–H stretching), 2511 cm^{-1} (S–H stretching), 1597 cm^{-1} (N–H bending of the amino group), and 1274 cm^{-1} (C–N stretching). Lastly, functional groups on the surface of HC-CQDs are explained by the peaks at 3232 cm^{-1} (O–H stretching), 1576 cm^{-1} (C═O stretching and N–H of the amino group), 1280 cm^{-1} (C–N stretching of amide), and 1094 cm^{-1} (C–O stretching).[45,46]

In the FT-IR spectra, HC-CQDs do not appear to exhibit a distinct S–H stretching vibration peak. This might be because the S–H stretching vibration peak in HC-CQDs is weak due to an inadequate C/N/S ratio. The identification of this peak is challenging. Thus, XPS methods were used for further analysis. The existence of S heteroatoms in HC-CQDs was confirmed by the

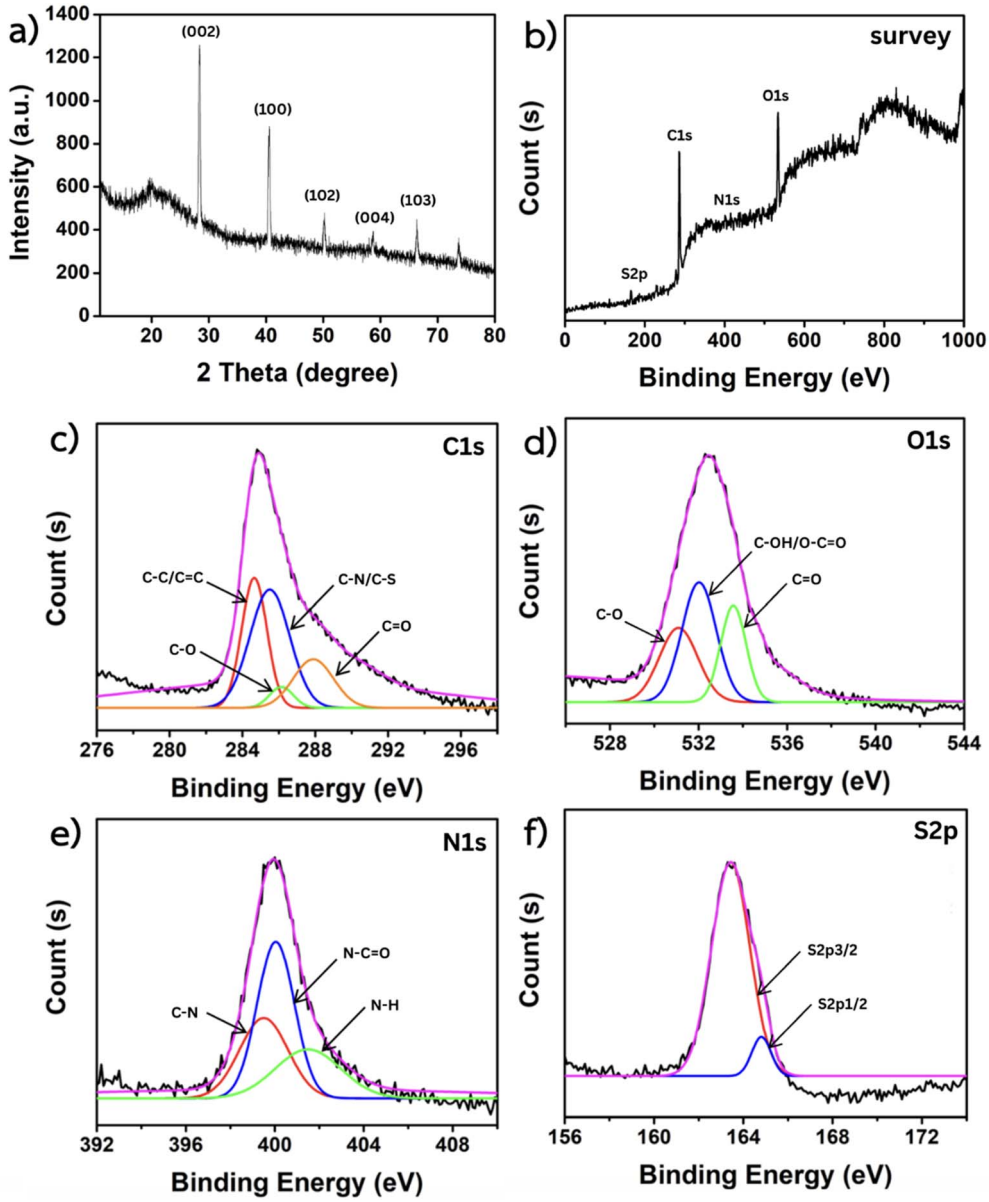

Fig. 3 (a) XRD patterns of HC-CQDs; (b) XPS survey spectrum of HC-CQDs; and (c–f) high-resolution XPS spectra of (c) C 1s, (d) O 1s, (e) N 1s, and (f) S 2p, respectively.

discovery of a peak of S 2p in the XPS survey spectra of HC-CQDs, which was located at 163.4 eV.

3.3 Crystallinity and chemicals composition

The XRD technique is commonly applied to find out the crystallinity of CQDs. As shown in Fig. 3a, a broad peak at 21.34° indicated the formation of a disorganized amorphous carbon.[47] The peaks at 28.39°, 40.11°, and 50.02° are attributed to the (002), (100), and (102) planes of graphitic carbon, respectively.[48,49] In addition, the weak peaks at 59.22° and 66.78° may be distorted peaks corresponding to the (004) and (103) planes of the crystalline carbon lattice, respectively.[50] Functional groups present on the surface of HC-CQDs may account for these distortions, which may indicate a higher degree of amorphous nature and the interaction of carbon with oxygen, which functions as a dopant due to its abundance in the plant extract.[51]

To confirm the chemical composition of HC-CQDs, XPS was utilized to analyze their elemental bonding. As shown in Fig. 3b, the survey spectra of HC-CQDs indicate four typical peaks at 163.4, 284.6, 399.5 and 532.0 eV which correspond to S 2p, C 1s, N 1s, and O 1s, respectively.[52] The high-resolution C 1s spectra shown in Fig. 3c were deconvoluted into four peaks, which

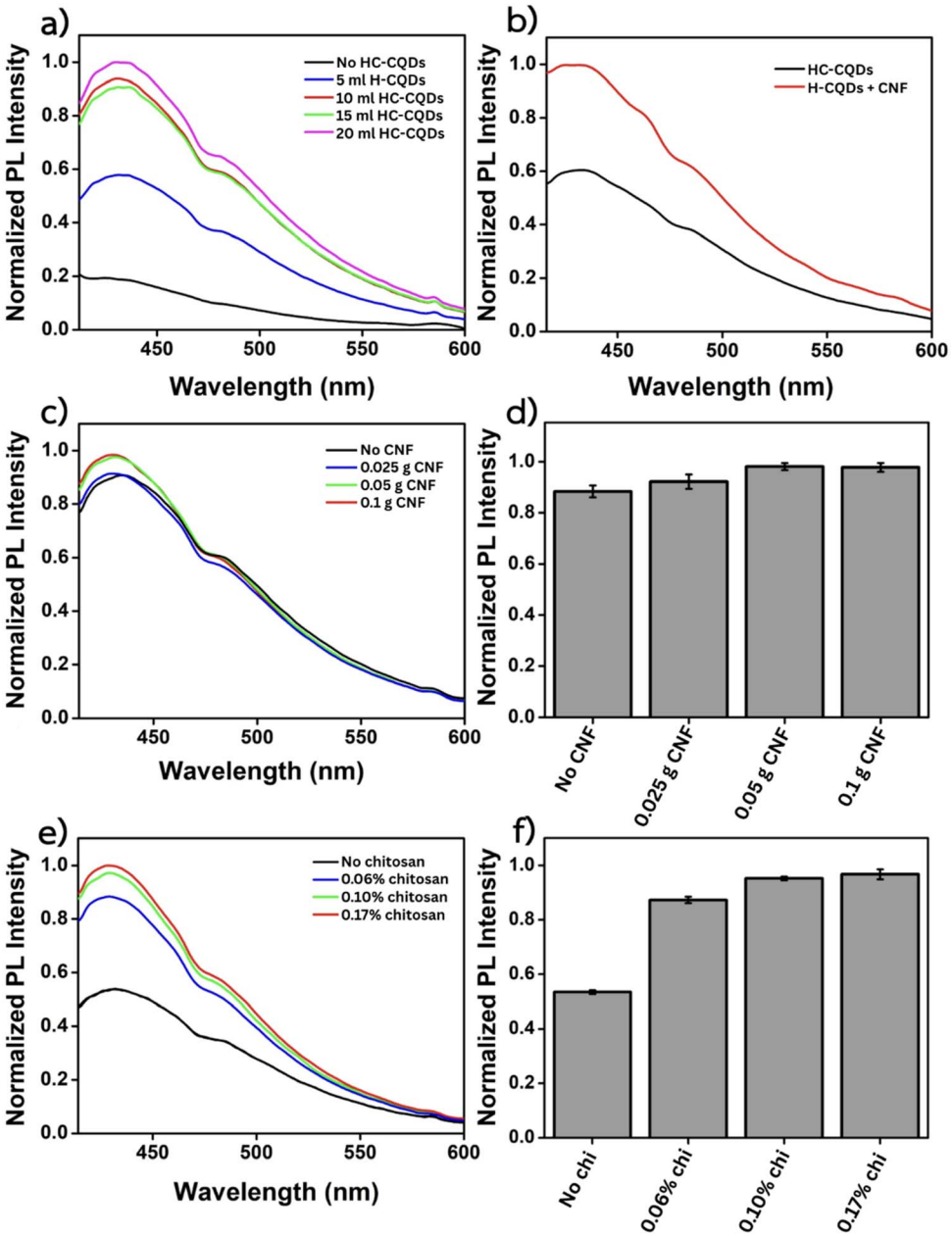

Fig. 4 (a) Emission spectra of HC-CQDs/starch powders with varying amounts of HC-CQDs; (b) comparison of the emission spectra between the HC-CQDs/starch and HC-CQDs-CNF/starch powders; (c) emission spectra and (d) corresponding bar graph of HC-CQDs-CNF/starch powders with varying amounts of CNF; and (e) emission spectra and (f) corresponding bar graph of the HC-CQDs-CNF-Chi/starch powders with different concentrations of chitosan.

indicate the type of bond and chemical structure of the carbon in HC-CQDs. The C–C/C=C bonds of graphitic sp^2 carbons are represented by the peak at 284.6 eV, C–N/C–S bonds by the peak at 285.5 eV, C–O bonds of hydroxyl carbons by the peak at 286.1 eV, and C=O bonds of carbonyl carbons[53] by the peak at 287.8 eV. The O 1s spectra in Fig. 3d indicate that the C–O bonds, C–OH/O–C=O bonds of carboxyl carbons, and C=O bonds are responsible for the three peaks at 531.1, 532.0, and 533.5 eV, respectively.[54] For the three peaks in the N 1s spectra shown in Fig. 3e, the C–N bonds are represented by the peak at 399.5 eV, N–C=O bonds by the peak at 400.3 eV, and N–H bonds of the amino group55 by the peak at 401.5 eV. Lastly, the S 2p spectrum (Fig. 3f) shows two peaks at 163.4 eV and 164.8 eV, corresponding to the C–S (thiophenic S, S $2p_{3/2}$) and C–S (thiophenic S, S $2p_{1/2}$) bonds, respectively. The results mentioned above confirm the presence of hydroxy groups (–OH), carboxyl groups (–COOH), sulfhydryl groups (–SH), and amino groups ($–NH_2$) on the HC-CQD surface.[55,56]

3.4 Preparation of the fluorescence fingerprint powder from HC-CQDs

To study the effect of the amount of HC-CQDs on the luminescence efficiency of the fluorescent powder, we measured the solid PL intensity of the fluorescent powder using different amounts of HC-CQDs. The preparation used cassava starch mixed with various amounts of HC-CQDs solution. Then, the mixture was dried, ground into a powder, and filtered through a sieve with 150-micron holes. Finally, the HC-CQDs/starch powder was obtained with a light yellow colour. From the results shown in Fig. 4a, the PL intensity of the fluorescent powder added with HC-CQDs increased with an increase in the volume of HC-CQDs. Cellulose nanofiber (CNF) was added to HC-CQDs-CNF/starch powder to enhance the PL performance of the fluorescence powder,[57] as shown in Fig. 4b. The fluorescent powder was synthesized as previously mentioned using three ingredients: tapioca starch, HC-CQDs solution, and CNF. Fig. 4c and d shows that the PL intensity of the fluorescent powder combined with HC-CQDs increases with the increase in the CNF volume. Chitosan was used as one of the components for synthesizing the fluorescent powder, and enhanced its adhesion to fingerprints on various material surfaces.[58] The HC-CQDs-CNF-Chi/starch powder was prepared by adding 0.5%w/v chitosan (in 0.1%v/v CH_3COOH) at various concentrations. The PL intensity of the HC-CQDs-CNF-Chi/starch powder had similar values and slightly increased with increasing chitosan solution concentration, as seen in Fig. 4e and f. Thus, the components of the HC-CQDs-CNF-Chi/starch powder (which include 20 mL of HC-CQDs solution, 0.01 g of CNF, and 5 mL of 0.5%w/v chitosan) are suitable components for detecting LFPs on various surface materials.

3.5 Latent fingerprints detection of the HC-CQDs-CNF-Chi/starch powder under normal and UV light

In this section, LFP detection on various surfaces was investigated. The HC-CQDs-CNF-Chi/starch powder was applied using both sprinkling and dusting methods. This powder was brushed onto different materials, including clear acrylic and stainless-steel surfaces. The surfaces were then exposed to UV light (365 nm) and photographed. As shown in Fig. 5a and b, fingerprints with clear and well-defined lines were obtained. In contrast, the HC-CQDs-CNF/starch powder (without chitosan) adhered to both the fingerprint and the surface (Fig. 5c and d), resulting in unclear fingerprints. This difference is attributed to the structure and properties of chitosan, which enable the fluorescent powder to selectively adhere only to the fatty and sweaty areas of fingerprints, leaving the material surface clean.

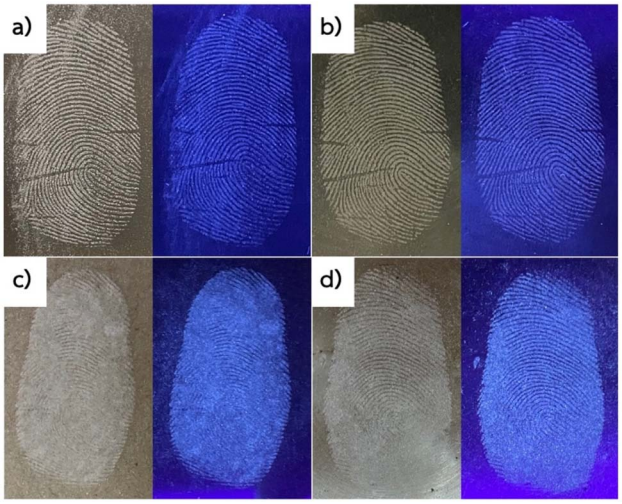

Fig. 5 Photographs of latent fingerprint (LFP) detection using different fluorescent powders on various surfaces under ambient (left) and UV light (right): (a) HC-CQDs-CNF-Chi/starch powder on a clear acrylic surface; (b) HC-CQDs-CNF-Chi/starch powder on a stainless-steel surface; (c) HC-CQDs-CNF/starch powder on a clear acrylic surface; and (d) HC-CQDs-CNF/starch powder on a stainless-steel surface.

3.6 Adhesion and interaction mechanisms of the HC-CQDs-CNF-Chi/starch powder with latent fingerprints

The interaction between LFPs and the HC-CQDs-CNF-Chi/starch powder, which mainly occurs through physical adhesive force, is explained in Fig. 6. The fluorescent powder is solid and dry. When it encounters a fingerprint that is moist, it will absorb and adhere to all areas where the fingerprint is. Human fingerprints can be printed on any material because the fingers are coated with sweat and grease. When fingers touch materials or surfaces, they will also retain fingerprint marks. As shown in Table S2, the zeta potential of synthesized HC-CQDs has a negative charge. Chitosan in the solid state has no charge. However, when it is dissolved in an acid solution such as acetic acid, the chitosan structure becomes positively charged.[59] When chitosan is mixed with CNF, cassava starch and HC-CQDs, the overall charge of the HC-CQDs-CNF-Chi/starch powder is positive. In addition to the physical adhesive force, other interactions between LFPs and the HC-CQDs-CNF-Chi/starch powder have been observed. This is likely due to the presence of positive charges of $-NH_3$ groups on the surface of the HC-CQDs-CNF-Chi/starch powder. When the FL powder encounters substances

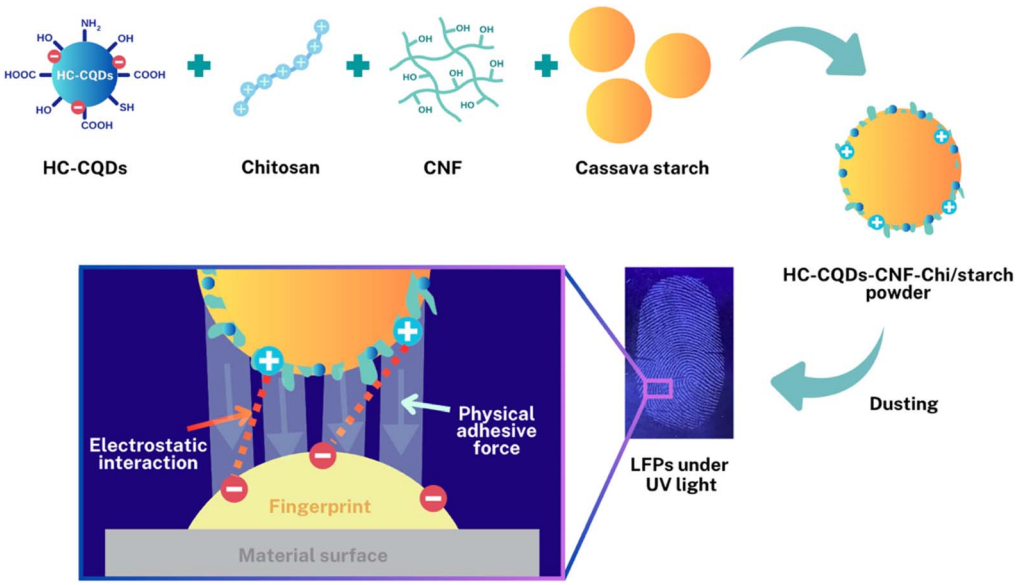

Fig. 6 Schematic of the interaction mechanism between latent fingerprints and the HC-CQDs-CNF-Chi/starch powder.

that are components of fingerprints (which are fatty acids and nucleic acids that have a negative charge), other interactions such as electrostatic interaction, hydrophobic interaction, and chemical reactions among functional groups occur.[60]

3.7 Latent fingerprints detection of HC-CQDs-CNF-Chi/starch powder under normal and UV light on different surfaces

To investigate the optical stability of the HC-CQDs-CNF-Chi/starch powder, fingerprints were developed using the powder on two non-porous surfaces: a clear acrylic surface and a stainless-steel surface. These samples were then placed at room temperature and exposed to UV light for different periods of time: 1, 7, 14, and 21 days. The results were as shown in the picture (Fig. 7). The results showed that over time, the glowing dust HC-CQDs-CNF-Chi/starch powder still possessed good fluorescence performance. It also adhered well to fingerprints. The printed fingerprints can be displayed clearly. Additionally, the effect of temperature on the optical stability of HC-CQDs-CNF-Chi/starch powder was studied. The fingerprints dusted by with HC-CQDs-CNF-Chi/starch powder was stored at various temperatures at 4 and 60 °C, and then exposed under UV light for different periods of time (1, 7, 14, and 21 days). The results presented in Fig. 7a and b from the experiment demonstrate that the glowing dust HC-CQDs-CNF-Chi/starch powder exhibits good adhesion to fingerprints over time. However, collecting fingerprinted material and storing HC-CQDs-CNF-Chi/starch powder for a long time may slightly decrease the

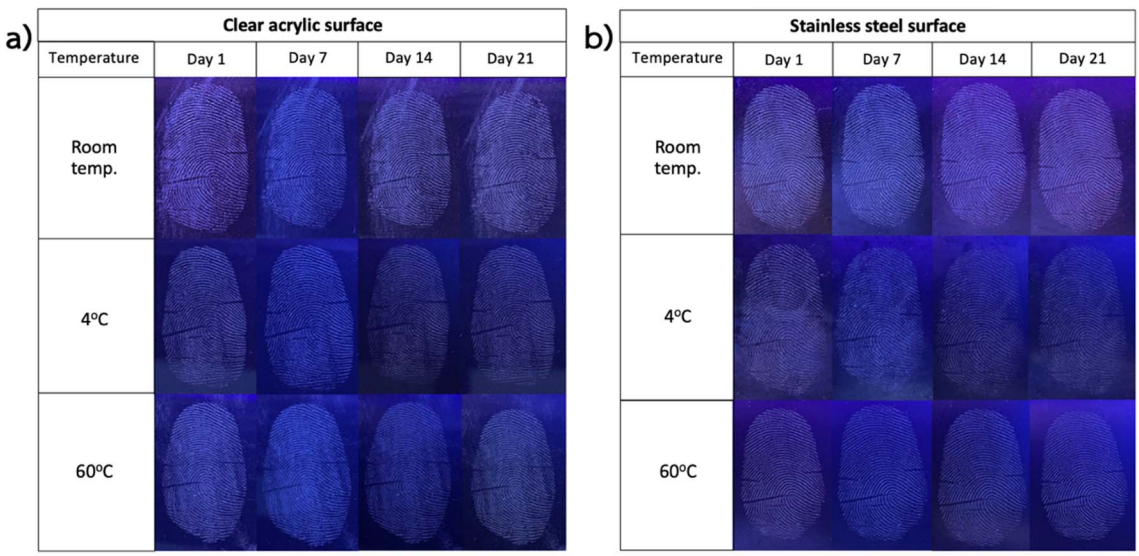

Fig. 7 Photographs showing the effect of storage temperature on latent fingerprint detection using HC-CQDs-CNF-Chi/starch powder on (a) a clear acrylic surface and (b) a stainless-steel surface.

luminescence efficiency of the HC-CQDs-CNF-Chi/starch powder.

3.8 HC-CQDs-CNF-Chi/starch powder for latent fingerprints detection: revealing ridge patterns

To investigate the detailed information of the ridge pattern, as depicted in Fig. 8a–e, successful detection of an LFP is achieved across all substrates. Fingerprint patterns can be divided into three main types: curved, rattan, and clamshell. The distinct ridge patterns of the LFP samples are easily discernible due to the heightened contrast of the fluorescent signals by the ability of the HC-CQDs-CNF-Chi/starch powder to adhere well to fingerprints, as depicted in Fig. 8a, which makes the fingerprints clearly visible and reveals the right loop pattern of the fingerprint.[61] Minutiae analysis is a more in-depth version of fingerprint analysis, which has a pattern and position on the fingerprint that is unique to each person.[62] Fig. 8b shows the minutiae called "crossover", which is a characteristic where two fingerprint lines form when two ridges cross each other. Fig. 8c demonstrates two types: ridge ending (1) and dot (2), which correspond to the fingerprint lines ending suddenly and the fingerprint lines that are so short they can be compared to a point, respectively. In Fig. 8d, the fingerprint is slightly longer than dots and occupies a middle space between two diverging ridges, which is a characteristic of an island pattern. Fig. 8e shows a ridge bifurcation, which has the characteristics of the lines at the point where a single ridge branches out into two or more ridges.[63]

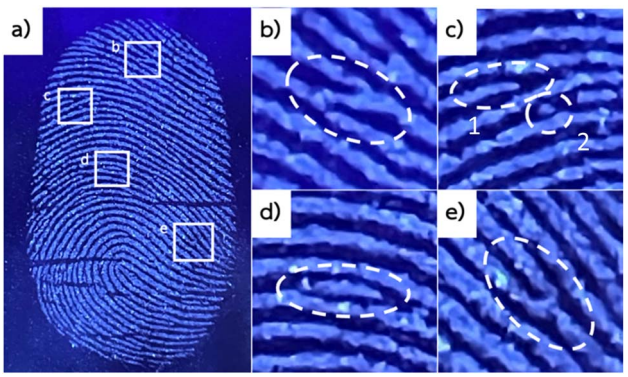

Fig. 8 (a) HC-CQDs-CNF-Chi/starch powder applied on a latent fingerprint on a stainless-steel surface under UV light, showing magnified minutiae details of (b) crossover; (c) ridge ending (1) and dot (2); (d) island; and (e) ridge bifurcation.

3.9 Effect of HC-CQDs on the viability of a cancer cell line after 48 h and 72 h exposure

HC-CQDs were evaluated for biocompatibility using the A549 lung adenocarcinoma cell line, SCC head and neck squamous carcinoma cell line, and LS174T colorectal cancer cell line (Fig. 9a–d). HC-CQDs were used with the MTT assay to determine the viability of the Vero kidney epithelium cell line in comparison to three cancer cell lines. The results showed that

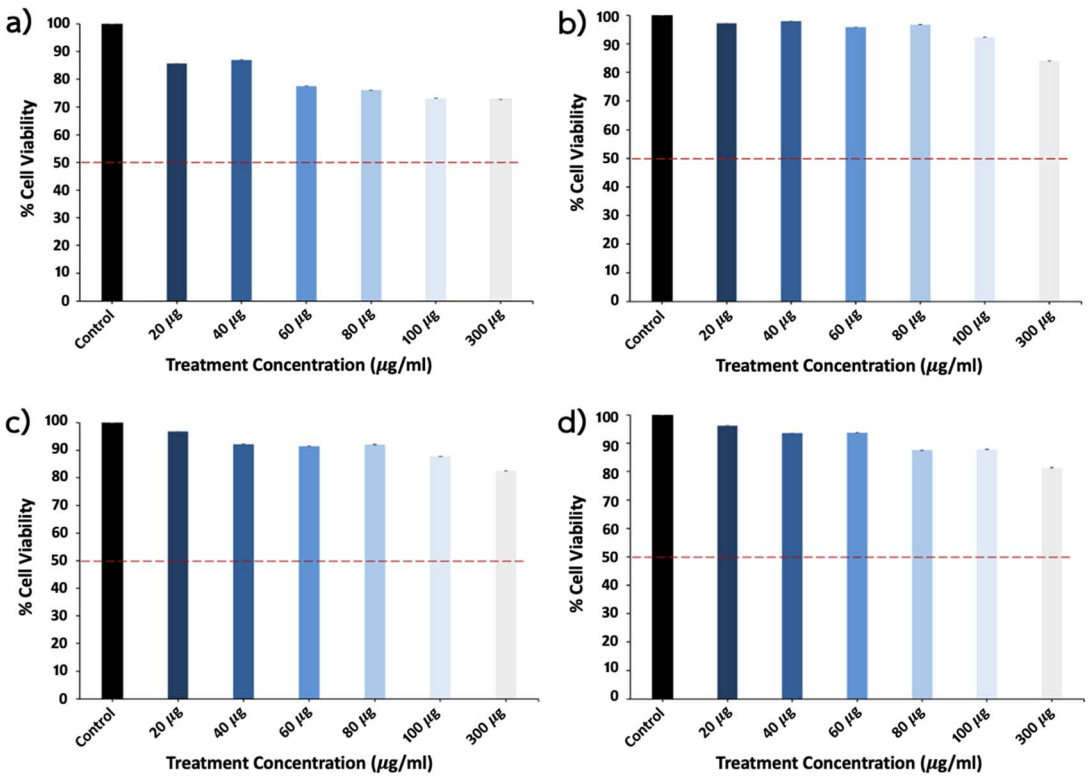

Fig. 9 Effect of HC-CQDs on the cell viability of various cancer cell lines and normal cells (Vero cells) after 48 hours of exposure. (a) A549 lung adenocarcinoma cells; (b) SCC head and neck squamous carcinoma cells; (c) LS174T colorectal cancer cells; and (d) Vero kidney epithelial cells. Data represent the mean ± standard error of the mean (S.E.M.) from three independent experiments ($n = 3$).

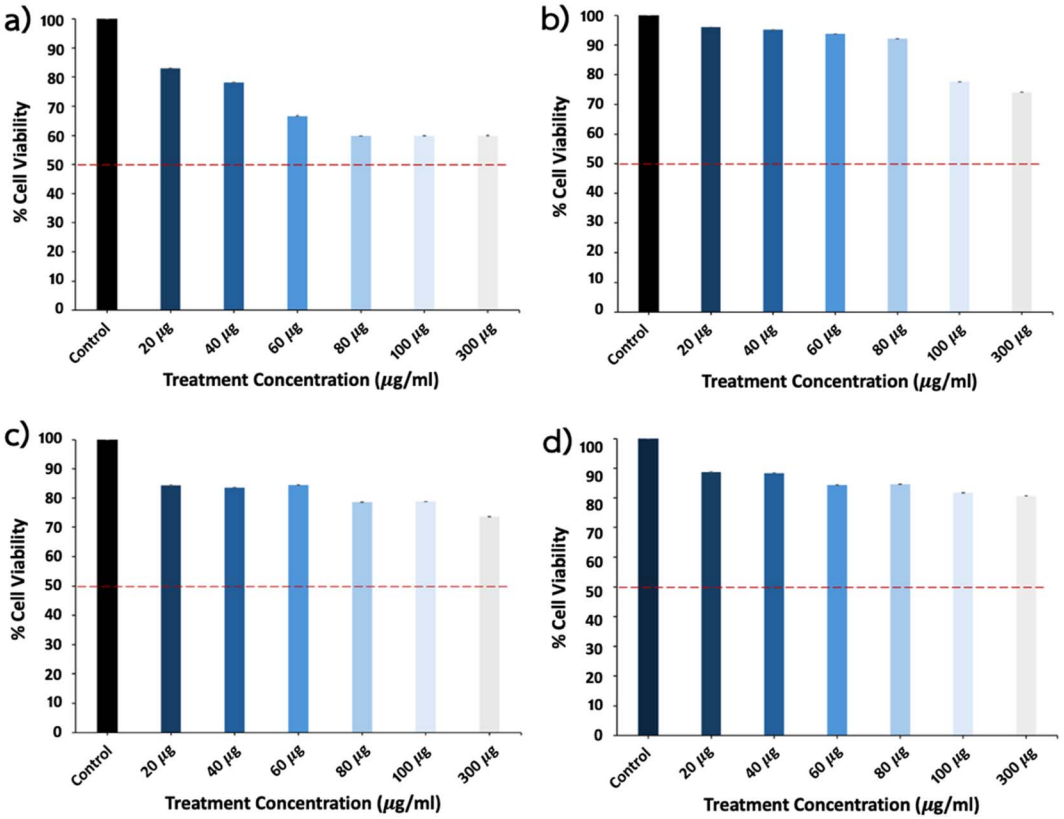

Fig. 10 Effect of HC-CQDs on the cell viability of various cancer cell lines and normal cells (Vero cells) after 72 hours of exposure. (a) A549 lung adenocarcinoma cells; (b) SCC head and neck squamous carcinoma cells; (c) LS174T colorectal cancer cells; and (d) Vero kidney epithelial cells. Data represent the mean ± standard error of the mean (S.E.M.) from three independent experiments ($n = 3$).

HC-CQDs reduced the A549 cell viability without significantly affecting the SCC, LS174T cancer cells and normal (Vero) cells after 48 h treatment with serial concentrations of HC-CQDs (20–300 μg mL^{-1}).

HC-CQDs were also characterized for their effect on the viability of cancer cell lines (A549, SCC and LS174T cells) and normal cell lines (Vero cells) for a longer incubation time (72 h). After treatment with HC-CQDs at various concentrations for 72 h, the cell viability of the cancer and normal (Vero) cell lines was analyzed. The results found that HC-CQDs treatment significantly reduced the viability of A549 cells with the maximal effect (~40% inhibition) being observed at 80 μg mL^{-1} (Fig. 10a). HC-CQDs also reduced the SCC and LS174T cell viability with weaker activity compared with A549 cells. The viability of the Vero cells was not affected after 72 h of HC-CQDs treatment (Fig. 10d). These results indicate that HC-CQDs exerted cytotoxic effects in A549 lung adenocarcinoma cells, with less activity being observed in SCC head and neck squamous carcinoma cells and LST174T colorectal cancer cells. HC-CQDs had no cytotoxicity effect on Vero kidney epithelium cells.

This work provides a preliminary result for the biological properties of HC-CQDs in inhibiting the activity of cancer cells. It was found that the synthesized HC-CQDs in this work were able to inhibit the activity of A549 cells with insignificant effect on normal cells and other types of cancer cell lines. More in-depth studies may be conducted to confirm their efficacy and safety in medical use. It is speculated that the mechanism of HC-CQDs in inhibiting only A549 cells may be that HC-CQDs may show specific toxicity to the A549 lung cancer cells owing to many factors, such as response to oxidative stress (ROS), interactions with cell membranes, cell membrane permeability, and sensitivity to cell death induced by CQDs,[64–66] which is a characteristic of A549 cancer cells that differs from normal cells or other cancer cells.

4. Conclusions

In summary, we have created highly fluorescent CQDs using hemp leaves and cysteamine hydrochloride. The synthesized HC-CQDs showed strong fluorescence intensity and stability with a high quantum yield of 36.1%. HC-CQDs were applied as an efficient fluorescent powder to detect LFPs, and they showed a high ability to easily distinguish the ridge patterns of the LFPs samples and clearly displayed visible fingerprints. The LFPs images can be used to analyze patterns and minutiae in fingerprints, which are considered useful information in identifying individuals. In addition, HC-CQDs possessed anti-cancer activity, especially in A549 lung cancer cells, but had no effect on normal (Vero) cells. The results indicate that our synthesized fluorescent fingerprint powder is safe for users. HC-CQDs would lead to efficiency in the production of fluorescent fingerprint powders for use in LFPs detection and help to provide valuable insights in forensic fields. Additionally, these

HC-CQDs might be turned into a tool for tracking cancer cells, using the same method to both detect lung cancer and provide treatment medications in the future.

Author contributions

Conceptualization, S. K., R. K., A. S., W. O., S. B., and C. M.; methodology and validation, R. K., A. S., W. O., W. S. T. T., C. M., K. M., C. S., P. S., W. S., S. B., and S. K.; formal analysis and investigation, S. K., R. K., A. S., W. O., C. M., P. S.; writing and preparing the first draft, R.K., S. K., C. M., and P. S.; authoring, reviewing, and editing, project management, supervision, and visualization, S. K., W. S. T. T, C. M., K. M., S. B., and R. K. The published version of the manuscript has been read and approved by all the authors.

Conflicts of interest

There are no conflicts to declare.

Data availability

The datasets generated and analyzed during the current study are available from the corresponding author upon reasonable request.

Supplementary information contains emission spectra, quantum yield data, zeta potential, particle size, EDX and H-NMR spectra of HC-CQDs. See DOI: **https://doi.org/10.1039/d5na00264h**.

Acknowledgements

Thanks for the financial support from the Center of Excellence for Innovation in Chemistry (PERCH-CIC), Ministry of Higher Education, Science, Research and Innovation. Laboratories and financial support of the Materials Chemistry Research Center (MCRC), Department of Chemistry, Faculty of Science, and Faculty of Science, Khon Kaen University, Thailand, are acknowledged. We are thankful for the XPS measurements by Miss Chomponoot Suppaso at the Department of Chemistry, School of Science, Institute of Science Tokyo, Japan. K. M. acknowledges the financial support from JSPS KAKENHI (grant numbers JP22H05142 and JP22H05148). C. M. acknowledges grants from the NSRF *via* the Program Management Unit for Human Resources & Institutional Development, Research and Innovation (grant number B05F650041) and the postdoctoral grant, Mahidol University, Thailand. The authors are also thankful for the TEM measurements by Mr Anuchit Rueangwitthayanon at Synchrotron Light Research Institute (Public Organization), Nakhon Ratchasima, Thailand.

References

1 S. Noureen, H. Jianfeng and F. Yongqiang, *Carbon Lett.*, 2022, **32**, 81–97.
2 V. Anuja, P. Tejaswini, G. Rutuja and P. T. Arpita, *Appl. Surf. Sci. Adv.*, 2022, **11**, 100311.
3 Z. Pinhui, S. Xiaoqing, D. Mingliang, S. Haiming, W. Wenxin, Z. Rui, S. Min and Z. Xingchi, *Constr. Build. Mater.*, 2022, **320**, 126312.
4 P. Mingfei, X. Xiaoqian, L. Kaixin, Y. Jingying, H. Liping and W. Shuo, *Nanomaterials*, 2020, **10**(5), 930.
5 E. P. M. De Meijer, M. Bagatta, A. Carboni, P. Crucitti, V. M. C. Moliterni, P. Ranalli and G. Mandolino, *Genetics*, 2003, **163**, 335–346.
6 W. Jiafeng, O. Wenjing, C. Gonglin, Y. Song, J. Chunyu, D. Guanghui, S. Hussain, P. Zhili and T. Kailei, *Ind. Crops Prod.*, 2025, **223**, 120146.
7 S. Raina, A. Thakur, A. Sharma, D. Pooja and A. P. Minhas, *Mater. Lett.*, 2020, **262**, 127122.
8 J. Asta, G. Rasa and B. Jurga, *Molecules*, 2023, **28**(13), 4928.
9 V. B. Harm, M. J. Stout, G. C. Atina, M. T. Carling, G. S. Andrew, R. H. Timothy and E. P. Jonathan, *Genome Biol.*, 2011, **12**, 02.
10 P. Jiying, Z. Hui, W. Xiaolei, Z. Hanchang and Y. Xiurong, *Anal. Chim. Acta*, 2012, **757**, 63–68.
11 S. B. Gurvinder, *Egypt. J. Forensic Sci.*, 2017, **7**, 4.
12 R. Ramotowski, H. C. Lee and R. E. Gaensslen, *Advances in Fingerprint Technology*, 2001, pp. 63–104.
13 P. Boonyaras, S. Boonpang and K. Dangudom, *J. Phys.: Conf. Ser.*, 2023, **2653**(1), 012075.
14 K. Nitin and P. K. Purnima, *J. Biomet. Biostat.*, 2011, **2**(4), 1000123.
15 P. Eswaran and P. Kriveshini, *J. Mater. Res. Technol.*, 2021, **12**, 1856–1885.
16 M. Snehasis, D. Kaustav, C. Sujan, S. Panchanan, K. Sudip, P. Mrinal, B. Asim and K. G. Chandan, *ACS Omega*, 2023, **8**(5), 4566–4577.
17 P. Mehrab, M. S. Salar, A. Hamidreza, A. Zeinab, A. Majid, R. Abbas and P. Sadanand, *BioNanoScience*, 2024, **14**, 4570–4584.
18 C. Mounika, S. Kondi, G. Sumanta, B. Aishwarya, S. Tanvi, S. B. Srivalliputtur, S. P. Vani, A. Somasundaram, V. Ravichandiran, M. Y. Murali and K. Govinda, *Nanotheranostics*, 2024, **8**(4), 442–457.
19 H. Amir, E. Hamid and R. N. Seyed, *ACS Omega*, 2023, **8**(23), 20987–20999.
20 A. Bayazeed, M. Tarun, K. Y. Sanjeev and S. P. Avanish, *ChemistrySelect*, 2022, **7**(48), e202204562.
21 V. M. Johan, J. L. K. Gertjan and C. Jacqueline, *Cancer Cell Culture*, 2011, **731**, 237–245.
22 S. Harpreet, B. Amy, K. Madhu and B. Neha, *Mater. Today: Proc.*, 2020, **28**, 1891–1894.
23 J. Carvalho, L. R. Santos, J. C. Germino, J. T. Ailton, A. M. J, J. Q. Fernando and G. F. Renato, *Mater. Res.*, 2019, **22**(3), e20180920.
24 L. Shiying, S. Wei and G. Zhiqiang, *Chem. Soc. Rev.*, 2015, **44**(1), 362–381.
25 S. Aphinan, S. Chaiwat, S. Peeranut, K. Pongtanawat, W. Wanwitoo, P. Jakkapop, Y. Saran, P. Pattaraporn, R. Sakhon, L. Navadol, C. W. W. Kevin and S. Chularat, *IJMS*, 2022, **23**(9), 5001.
26 L. Xiaoming, Z. Shengli, A. K. Sergei, L. Yanil and Z. Haibo, *Sci. Rep.*, 2014, **4**(1), 4976.

27 T. Aschalew, H. Mebrahtu, R. Dharmasoth, B. Kaloth and B. Neway, *ACS Omega*, 2020, **5**(8), 3889–3898.
28 B. Fathalla, M. Mokhtar, H. Sherin, B. Aya and A. Hytham, *J. Fluoresc.*, 2021, **31**(1), 85–90.
29 D. Kandi, S. Mansingh, A. Behera, K. Parida and K. S. Dibyendu, *J. Lumin.*, 2021, **231**, 117792.
30 Z. Pei, Z. Qin, C. Juanjuan, Q. Cheng, Y. Jing, X. Situan, Z. Yonggui and L. Yanbin, *Nanomaterials*, 2022, **12**(9), 1528.
31 M. Lan, W. Wanting, H. Jialiang, P. Hao, S. Yingjin, S. Yutong, T. Junyu, C. Guanyi and Z. Zhihua, *Ind. Crops Prod.*, 2024, **219**, 119026.
32 W. Cunjin, S. Huanxian, Y. Min, Y. Yujia, L. E, J. Zhen and F. Jun, *Mater. Res. Bull.*, 2020, **24**, 110730.
33 L. Yang, L. Yanan, P. Mira, P. Soojin, Z. Yifan, A. Rashedunnabi, P. Byungyong and K. Hakyong, *Carbon Lett.*, 2017, **21**, 61–67.
34 R. Haitao, Y. Yue, L. Abdelkader, D. Qibing, Z. Ke, L. Eric, A. A. Ahmed, S. A. Jamaan and W. Chuanyi, *Chin. Chem. Lett.*, 2023, **34**(6), 107998.
35 Y. J. Sun, J. S. Tang, L. Xiang, X. Hu, J. Wei and X. J. Song, *Dig. J. Nanomater. Biostruct.*, 2022, **17**(4), 1327–1343.
36 M. S. K. Zubair, S. R. Raja, A. Shumaila, I. Shama and Z. M, *Opt. Mater.*, 2019, **91**, 386–395.
37 R. Yi, I. N. W. Geoffrey and L. Siyu, *Aggregate*, 2022, **3**, e296.
38 B. Sourav, *J. Controlled Release*, 2016, **235**, 337–351.
39 F. D. Rute, A. B. Mohamed, Y. Jumam, M. R. M, T. Nathalie, R. L. Jamie, G. L. Gary and J. W. Kevin, *Environ. Sci. Technol.*, 2009, **43**(19), 7277–7284.
40 P. Pratibha, D. Geeta and J. Rabita, *Chem. Pap.*, 2024, **78**, 5993–6010.
41 L. Miyuan, M. Chuanjun, W. Guanlong, Z. Xiugang, D. Xiaoli and M. Hongchao, *Res. Chem. Intermed.*, 2021, **47**(8), 3469–3485.
42 Y. Byongyoug and K. Seungyeop, *J. Mater. Chem.*, 2012, **22**(17), 8345.
43 T. Mahnoush, T. Y. Mohammad, A. Mahnaz, T. Mohammadreza, V. Daryoosh and T. Lobat, *Colloid Polym. Sci.*, 2016, **294**(9), 1453–1462.
44 Y. Wei, H. Yingchen, Y. Zhihong, W. Chunxian, Z. Feiyan and L. Yi, *RSC Adv.*, 2021, **11**(57), 36310–36318.
45 A. M. N, A. F. Awatef, M. A. Hala and M. T. Aghareed, *Arab. J. Chem.*, 2018, **11**(4), 546–553.
46 R. Ludfiaastu, E. N. Reva, M. I. M. Rizky, C. Uswatul, W. Sayekti and H. R. Ari, *J. Chem. Pharmaceut. Res.*, 2015, **7**(6), 85–89.
47 C. Avinash, K. Aditya, P. Sandeep, V. D. B, M. R. Tanu and K. Venkataramaniah, *Mater. Focus*, 2016, **5**(1), 55–61.
48 A. Natarajan, R. Murugesan, S. Chellappan, S. Thangasamy, K. Ponnuchamy, L. Yunsung and K. S. Ramakrishnan, *Environ. Res.*, 2021, **199**, 111263.
49 G. N. Gaurav, B. A. Md, P. Vivek, M. Debadatta, K. D. Pawan, S. P. Avanish and N. S. Alakh, *J. Fluoresc.*, 2020, **30**, 407–418.
50 L. Yan, Z. Yang, C. Huhu, H. Yue, S. Gaoquan, D. Liming and Q. Liangti, *J. Am. Chem. Soc.*, 2012, **134**, 15–18.
51 Y. Shweta, T. Bothe, M. B. Santosh, R. S. Sapam, R. P. Sneha, S. Mika, G. M. J, G. S. J and B. Y. Ramesh, *Sci. Rep.*, 2024, **14**(1), 9915.
52 Z. Jin, W. Hong, X. Yiming, T. Ju, L. Changneng, L. Fengyan, D. Haiming and X. Wen, *Nanoscale Res. Lett.*, 2017, **12**(1), 611.
53 D. Yuanfei, Z. Feng, X. Jiacong, M. Yongzhen, L. Xuguang and X. Bingshe, *RSC Adv.*, 2017, **7**(46), 28754–28762.
54 K. Honghee, L. Yeonju, P. Chanho, Y. Seunggun, W. Sungok, S. Wonseon, P. Cheolmin and C. Wonkook, *Part. Part. Syst. Charact.*, 2018, **35**(7), 1800080.
55 L. Teng, C. Zhiwei, Z. Jun, W. Ying and Z. Zhigang, *Nanoscale Res. Lett.*, 2017, **12**(1), 375.
56 L. Kuan, *J. Fluoresc.*, 2019, **29**(3), 769–777.
57 P. Emilia, B. Douglas and M. G. William, *Cellulose*, 2019, **26**(8), 5117–5131.
58 K. Ono, Y. Saito, H. Yura, A. Kurita, T. Akaike and M. Ishihara, *J. Biomed. Mater. Res.*, 2000, **49**(2), 289–295.
59 S. Jeanne, D. Cédric, M. Philippe and D. B. Helene, *Polymers*, 2021, **13**(22), 4031.
60 C. Haobin, C. Kaiwen, M. Xiaoju, S. Kai, F. Xiaofeng, M. Chi, Z. Yongxi, Y. Shengyan, Q. Weiping and W. Changfeng, *ACS Appl. Mater. Interfaces*, 2015, **7**, 14477–14484.
61 D. Ritika, K. Mandeep and K. Manvjeet, *Egypt. J. Forensic Sci.*, 2021, **11**, 33.
62 U. D. Uttam, V. S. Malemath, M. P. Shivanand and V. C. Sushma, *Int. J. Inf. Tecnol.*, 2022, **14**(2), 1025–1039.
63 A. Wahaba, T. M. Khanb, S. Iqbalc, B. AlShammarid, B. Alhaqbanie and I. Razzak, *Procedia Comput. Sci.*, 2024, **246**, 1558–1567.
64 A. A. Stepanenko and V. V. Dmitrenko, *Gene*, 2015, **574**, 193–203.
65 S. Kavitha, M. Suganya, P. Ponnusamy, S. D. C. Catherine, L. D. Matthew, G. B. Mythili and P. Sudhagar, *ACS Appl. Nano Mater.*, 2018, **1**, 1683–1693.
66 E. E. Hossam and B. A. Hanan, *Int. J. Biol. Macromol.*, 2021, **170**, 688–700.